Transforming Wood into a High-Performance Engineering Material via Cellulose Nanocrystal Impregnation

Dilpreet S. Bajwa Ismat Ara Ashton Oriel Chan
Sreekala G. Bajwa Kerry E. Hartman

Abstract

The demand for wood in construction has led to shortages of strong wood types, causing a shift to costlier alternatives like concrete and nonbiodegradable materials, prompting the investigation of modifying softwoods for better engineering properties. This study investigates the optimization of a multistep impregnation process utilizing functionalized cellulose nanocrystals (f-CNCs) to enhance softwood properties. The process involves alkali delignification, ultrasonication, and vacuum pressure treatment to improve wood porosity and in turn improve CNC impregnation with uniform dispersion. Microstructural analyses through field emission scanning electron microscopy and atomic force microscopy (AFM) offer detailed insights into cell wall morphology and surface topography, whereas Fourier transform infrared spectroscopy highlights compositional shifts resulting from f-CNC impregnation. Mechanical testing demonstrates significant improvements for treated woods, particularly a 67 percent increase in modulus of elasticity for the 2 percent CNC-treated group compared with the control group; a 71 percent increase in modulus of rupture was observed for 2 percent CNC-, 3 percent NaOH-, and 2 percent acetic acid-treated group compared with the control sample. The sample delignified with 3 percent NaOH and impregnated by 2 percent f-CNC emerged as particularly effective. This research sets the stage for potential advancements in strengthening softwood using CNC, including a novel AFM method and alternative impregnation techniques like the Lowry method, inviting further exploration.

Wood is a renewable material with a wide range of applications and properties. However, the increasing demand for wood as a construction material has led to shortages in the availability of high-strength wood and the depletion of natural forests (Nepal et al. 2021). The diminished availability of aged trees for harvesting has led builders to resort to more expensive alternatives, such as concrete (Ameh et al. 2019). This situation has also led to the increased use of nonbiodegradable materials, such as plastic polymers (Brandner et al. 2016). To meet the demand for higher-strength wood products, softwood varieties that are not typically used for advanced applications can be modified to obtain desirable engineering properties.

Common methods for wood modification include delignification and densification. Delignification is a process that removes the lignin within the wood, a key structural material. However, because of the heterogeneous and complicated nature of lignin within the wood, along with its recalcitrance, removal of lignin can facilitate modification techniques by either increasing porosity of the wood or inducing the collapse of cell walls within the wood (Qian et al. 2019). On the other hand, densification requires the compression of wood to increase its density (Frey et al. 2018). Densification enhances the mechanical properties of wood by achieving a higher microstructural homogeneity while preserving structural directionality (Kollmann et al. 2012).

In addition, wood can be modified through impregnation of desired chemicals to induce desirable properties onto the wood, such as increased density, strength, and durability, depending on the species (Nikolic et al. 2015, Taghiyari et al. 2017). Impregnation is conducted in numerous ways, with the most common methods being full-cell and empty-cell treatments (Laks 2008). The full-cell method, or the Bethell method, induces an initial vacuum to remove air pockets in

The authors are, respectively, Professor (dilpreet.bajwa@montana.edu [corresponding author]), Postdoctoral Associate (ismat.ara@montana.edu), and Student (ashton.chan@student.montana.edu), Dept. of Mechanical and Industrial Engineering, Montana State Univ., Bozeman, Montana; Professor, College of Agric., Montana State Univ., Bozeman, Montana (sreekala.bajwa@montana.edu); and Sci. Chair/Academic Dean, Neuta Hidatsa Sahnish College, New Town, North Dakota (hartm@nhsc.edu). This paper was received for publication in September 2023. Article no. 23-00054.
©Forest Products Society 2024.
Forest Prod. J. 74(1):62–71.
doi:10.13073/FPJ-D-23-00054

http://prime-pdf-watermark.prime-prod.pubfactory.com/ | 2024-12-26

the wood. The vacuum is followed by a pressure treatment of the wood to fill the full wood cell with a desired chemical until desired chemical retention is obtained. This process yields maximum chemical retention by filling the lumen of the wood with the desired chemical (Rasouli et al. 2017). This is typically done when it is desirable for the preservative to be absorbed into the wood, regardless of penetration within the sample (Nikolic et al. 2015, Rasouli et al. 2017). On the other hand, the empty-cell method, also known as the Lowry method, uses compressed air to drive out a portion of the preservative absorbed during the pressure period while maintaining deep preservative penetration (Laks 2008, Sandberg et al. 2017). This is typically done with chemicals where penetration deep within the wood sample is desired (Sandberg et al. 2017, Taghiyari et al. 2017).

The effectiveness of these impregnation techniques can be improved using delignification because greater amounts of nanofiller can be inserted into the wood with increased porosity. Previous studies reported that the combination of delignification and complete cell impregnation in wood yielded enhanced mechanical properties (Taghiyari et al. 2017, Khakalo et al. 2020, Luo et al. 2022). The integration of delignification with an ionic liquid treatment in birchwood resulted in a significant improvement, leading to an increase in tensile strength from 70 to 375 MPa and an increase in Shore D Hardness from 53 to 82 (Khakalo et al. 2020). Additionally, it was reported that delignification combined with an empty-cell impregnation treatment using nanoaluminum oxide in poplar wood resulted in an increase in elastic moduli from 0.6 to 1.4 GPa (Taghiyari et al. 2017).

Various research studies have been done on wood impregnated with nanofillers such as nanoparticles, metal oxides, clays, and biobased materials to obtain desirable properties (Nikolic et al. 2015, Taghiyari et al. 2017, Luo et al. 2022). A relatively new biobased nanofiller (Luo et al. 2022) that is used for wood impregnation is cellulose nanocrystals (CNCs). Impregnation of CNCs can enhance the physical and mechanical properties of poplar wood (Luo et al. 2022). The CNCs are better than currently used inorganic nanofiller because of the biodegradable nature of the CNCs, and because CNCs can be sourced from marginal-value wood or wood products, such as pine chips (Habibi et al. 2010, Taghiyari et al. 2017). In addition, CNC is an extremely advantageous nanofiller to use because of its desirable mechanical properties, with a tensile strength of 7 GPa and an elastic modulus of 150 GPa (Chanda and Bajwa 2021); low cost at $4.89/kg (Rajendran et al. 2023); and tunable surface chemistry (Tang et al. 2013, Shojaeiarani et al. 2018).

As a result of the surface modification properties, these CNCs can be further strengthened via Fischer–Speier esterification using benzoic acid (BA) or acetic acid (AA; Tang et al. 2013, Shojaeiarani et al. 2018). BA and AA modify the surface of CNCs by introducing functional groups, allowing the conversion of surface hydroxyls into esters via Fisher esterification (Rana et al. 2021). This modification leads to the development of rough and irregular surfaces, fostering ductile fracture in the material. Consequently, when blended into polymers such as polylactic acid (PLA), this enhancement results in improved mechanical properties (Young's modulus increase from 3.33 to 4.23 GPa; Shojaeiarani et al. 2018). This highly tunable surface chemistry of CNCs can be exploited to further enhance the physical and mechanical properties of wood—a domain that remains largely unexplored on the basis of existing literature.

The current research aimed to design and test a novel method to impregnate functionalized CNCs (f-CNCs) into a marginal-quality softwood. The purpose of softwood f-CNC impregnation is to increase the value of softwood by enhancing its mechanical properties for advanced engineering and architectural applications to meet the rising demand of high-strength wood products (Brandner et al. 2016). So far only, nonfunctionalized CNCs have been used to impregnate wood to enhance its mechanical properties (Luo et al. 2022). However, current research hypothesizes that f-CNCs will further enhance the physical and mechanical properties of softwood. To test this hypothesis, the first objective was to optimize and validate an effective process of impregnating wood with f-CNCs and determine critical variables influencing CNC impregnation into the wood using delignification and a Bethell vacuum–pressure impregnation process. The second objective was to investigate the microstructural, physiological, and compositional changes in wood impregnated with CNC via field emission scanning electron microscopy (FESEM), atomic force microscopy (AFM), and Fourier transform infrared spectroscopy (FTIR). The third objective was to evaluate the physical and mechanical properties of f-CNC-impregnated wood through a series of ASTM D1037-12 and ASTM D2339-98 tests. The novelty of this research is that it uses f-CNCs to assess whether functionalization of CNCs is a viable method to enhance the physical and mechanical performance of wood compared with that of wood impregnated with untreated CNCs. The outcomes of this research can help the lumber industry to transform marginal timber into high-value and fast-growing wood.

Materials and Methods

Materials and chemicals

Southern yellow pine (SYP) was studied because of its low-cost and lightweight construction applications (Briggs 2010). Commercial SYP boards (6.35-mm thickness by 35-mm width) were sourced commercially from a local wood-products store. Sodium hydroxide (formula weight 40.00 g/mol) purchased from Fisher Chemical (Fair Lawn, New Jersey, USA) was used as a delignification agent. CNCs with dimensions of 10 to 15-nm width and 80 to 100-nm length and aspect ratios of 5 to 10 were provided by the US Department of Agriculture Forest Products Laboratory (Madison, Wisconsin, USA). These CNCs were extracted from softwood pulp via sulfuric acid hydrolysis and desulfated using hydrothermal treatment. The extracted CNCs were freeze-dried and kept in sealed bags. Glacial AA (molecular mass 60.05 g/mol) obtained from Fisher Chemical and BA pellets (formula weight 122.12 g/mol) obtained from Carolina Biological Supply Company (Burlington, North Carolina, USA) were used as grafting agents. Deionized (DI) water bought from Millipore (Burlington, Massachusetts, USA) was used as the solvent.

Design of experiments

All treatments consisted of combinations of individual treatments described in Table 1. Because of the multistep treatment process a full factorial design was implemented for the treatment of SYP to test four-factor effects: the effect of delignification, the effect of CNC impregnation at different concentrations,

http://prime-pdf-watermark.prime-prod.pubfactory.com/ | 2024-12-26

Table 1.—Treatment summary with a linear combination of factors.

Treatment	Factor levels
Sodium hydroxide (N)	% concentration of sodium hydroxide Two levels: 0 wt. %, 3 wt. %
Cellulose nanocrystals (CNCs)	% concentration of cellulose nanocrystals Four levels: 0 wt. %, 1 wt. %, 2 wt. %, 5 wt. %
Acetic acid (AA)	% concentration of acetic acid nanosuspension Two levels: 0 wt. %, 2 wt. %
Benzoic acid (BA)	% concentration benzoic acid nanosuspension Two levels: 0 vol. %, 2 vol. %
Unique formulation total	$2 \times 4 \times 2 \times 2 = 32$
Combined BA/AA removal	8
Unique formulation net total	$2 \times 4 \times 2 \times 2 - 8 = 24$
Example 1: 3N2AA2CNC	3 wt. % sodium hydroxide, 2 vol. % acetic acid, and 2 wt. % CNC sample treatment
Example 2: 5CNC	0 wt. % sodium hydroxide, 0 vol. % acetic acid, and 5 wt. % CNC sample treatment

the effect of BA functionalization of CNCs, and the effect of AA functionalization of CNCs. The experimental design started with 32 different flexural test treatments, as shown in Table 1, using a modified full-factorial design test. The flexural test determining modulus of rupture (MOR) and modulus of elasticity (MOE) are strong indicators of engineering performance in a sample. Because of the redundancies in the treatment combinations that went beyond the scope of this experiment, the number of treatments was reduced to a net total of 24 treatments for the flexural test. Concentrations were limited for certain treatments, such as acid suspension and delignification treatment, as they were used to understand the effect of each treatment, such as delignification and AA/BA surface functionalization of CNCs. Upon testing these treatments, the top six treatments obtained from the MOR and MOE results were selected for further physical and mechanical properties testing, which are described under "Physical and mechanical tests" subsection.

Treatment methodology of the SYP

The treatment process consisted of multiple steps, including the preparation of different CNC nanosuspensions, delignification of the SYP, ultrasonication of the SYP and nanosuspension, and vacuum–pressure treatment of the SYP and nanosuspension. The CNC nanosuspensions were developed to identify optimal surface modification agents. To create a nanofiller with highly desirable mechanical properties, surface grafting of CNCs using BA and AA was done using procedures reported in the literature (Shojaeiarani et al. 2018). BA pellets were pulverized via mortar and pestle and poured into a 300-mL solvent of DI water at 2 wt. percent. The BA solution was stirred at 600 revolutions per minute (rpm) and melted at 140°C for 4 hours on a stir plate to enhance solubility throughout the solvent. The BA solution was cooled for 45 minutes to prevent the melting of CNCs. CNC chunks were pulverized and added to the BA. The CNCs were stirred overnight at concentrations of 1, 2, and 5 wt. percent. For AA, glacial AA was poured into a 300-mL solvent of DI water at 2 vol. percent. The AA was stirred at 600 rpm for 5 minutes because of its high solubility. Chunks of CNCs were pulverized and added to the AA at 1, 2, and 5 wt. percent concentrations and stirred overnight.

Delignification was conducted using procedures as reported in the literature (Qian et al. 2019) and optimized for SYP to facilitate lignin removal and the collapse of cell walls during vacuum–pressure treatment. A 300-mL, 3 wt. percent NaOH solution was stirred at 600 rpm in a low-density polyethylene container and heated to 80°C on a hot plate. Ten strips of SYP were immersed using glass beakers. The SYP was immersed for 2.5 hours and removed for drying. The wood was dried on an oven rack at 70°C overnight before additional testing or treatment. Dried SYP strips were placed into a thermos and separated using a PLA disk with 10 slots. The (BA or AA) grafted CNC was poured into the thermos and rested for 15 minutes. The SYP strips were then ultrasonicated for 25 minutes at 18 kHz in a Hielscher UIP1000hdT ultrasonicator (Berlin, Germany) to ensure even dispersion of the CNC nanosuspension and minor impregnation throughout the SYP samples (Kargarzadeh et al. 2017).

Ultrasonicated SYP strips encased within a thermos were inserted into the vacuum–pressure vessel. The vessel was designed to hold an 80-kPa vacuum and 800-kPa pressure to impregnate the surface-grafted CNC solution into the samples. Vacuum–pressure was applied for 100 minutes and subsequently the positive pressure was continued for 120 minutes. The times selected for the vacuum–pressure treatment and the pressures applied were based on preliminary results under a light microscope visually maximizing impregnation. The vacuum was applied using a Rocker 410 vacuum pump and pressurized using an 800-kPa air hose attached to the laboratory building.

Characterization

Field emission scanning electron microscopy.—Topographical and elemental information were obtained using Supra 55VP FESEM (Zeiss, Thornwood, New York, USA) operated at an accelerating voltage of 15.0 kV within the facilities of the Image and Chemical Analysis Laboratory at Montana State University. In this study, FESEM was used to analyze especially the cell walls of the material. However, the disadvantages of FESEM are that it only produces surface images and chemical composition in specific modes (Reza et al. 2015, Abraham et al. 2020). This method cannot assess surface-level mechanical properties, which may pose problems with materials containing similar morphologies, such as wood and CNCs.

Atomic force microscopy.—This study used AFM to provide details of SYP topography and detect CNCs within a localized area (1 by 1 μm). A Cypher S (Asylum Research, Santa Barbara, California, USA) AFM was used with Bruker RTESPA-525 probes (spring constant: 200 N/m, resonance

http://prime-pdf-watermark.prime-prod.pubfactory.com/ | 2024-12-26

frequency: 525 kHz). Surface topography was mapped using tapping mode, where the AFM cantilever oscillates at or close to its resonance frequency near the sample's surface. Modulus maps were collected using the fast-force mapping mode of the instrument, which rapidly collects ~300 force-displacement curves per second, as the probe rasters back and forth across the desired sampling area. To extract a material modulus value from each force-displacement curve, each pixel was fit with a Hertzian contact mechanics model. The Hertzian contact mechanics model simulates a sphere rolling onto a flat surface, as shown in Equation 1. Modulus maps of 1 μm^2 with a pixel size of 256 allowed a pixel resolution of 3.9 nm. Modulus maps were generated using the Hertzian contact model, assuming a sphere is rolling onto a flat surface. The calculation for the Hertzian contact model is as follows:

$$F = \frac{2E\tan(\alpha)}{\pi(1-\nu^2)\delta^2} \quad (1)$$

where the force F is represented as a function of the indentation (δ), Young's modulus (E), tip opening angle ($\alpha = 35°$), and the Poisson ratio (ν; assumed to be 0.5 considering for soft material).

Fourier transform infrared spectroscopy.—FTIR was used to analyze the chemical composition of the SYP impregnated with f-CNCs using a Thermo-Scientific FTIR/attenuated total reflectance (ATR) spectrometer, model Nicolet iS50 (ThermoFisher Scientific, Madison, Wisconsin, USA). An ATR ID7/ITX AR-coated diamond crystal was used for the purpose of the FTIR experiments. The motivation for using FTIR was to determine and compare the chemical composition of f-CNC-treated and untreated SYP and see the resulting chemical changes in the functional groups due to hydrogen bonding resulting from CNCs and f-CNCs when impregnated into wood. The spectra resulted from 32 times averaged scans at five different points across the sample and were acquired at a resolution of 4 cm^{-1} from 400 to 4,000 cm^{-1}. The background spectra, i.e., the data without the sample loaded, was taken as well; subsequently the background was subtracted from each FTIR data set to get baseline correction.

Physical and mechanical tests

Density.—To evaluate the impregnation rate of SYP via CNCs, the relative change in density ($\Delta\rho$) was measured, as displayed in Equation 2. Five wood strips (6.35 mm in thickness, 17.5 mm in width, and 180 mm in length) were dried at 70°C for 10 hours and weighed and measured both before treatment and after treatment.

$$\Delta\rho = \frac{\rho_t - \rho_0}{\rho_0} \times 100\% \quad (2)$$

where $\Delta\rho$ is the percent change in density, ρ_0 is the density before treatment, and ρ_t is the density after treatment.

Water absorption, thickness swelling, and linear expansion.—ASTM D1037-12 (ASTM 2018a) was followed for water absorption, thickness swelling, and linear expansion measurement. To determine the liquid absorptiveness and resilience properties of SYP, water absorption tests were conducted. Each of the five SYP strips of 6.35 by 17.50 by 180 mm was weighted, submerged in 25 mm of water for 24 hours in a polypropylene container, and dried for 10 minutes. Resulting masses of the samples were measured, and the moisture absorption was calculated on the basis of following equation:

$$\mathrm{WA}\,\% = 100 \times \frac{m_w - m_d}{m_d} \quad (3)$$

where WA% is the water absorption, m_w is the mass of the sample when wet, and m_d is the mass of the sample after drying.

To measure the hygroscopic properties of SYP, thickness swelling tests were conducted. The same strips and submersion procedure were used as water absorption tests, with the only difference being the thickness measurement was considered before and after submersion instead of weight.

Linear expansion tests were conducted to measure SYP's dimensional stability in atmospheric humidity. Five strips of SYP with dimensions of 6.35 by 17.50 by 180 mm were inserted into an ESPEC EPL-4H temperature humidity chamber (Hudsonville, Michigan, USA) at 50 percent humidity for 24 hours and then at 90 percent humidity for 24 hours. The percent difference in length was calculated using the following equation:

$$L_e = 100 \times \frac{L_{90} - L_{50}}{L_{90}} \quad (4)$$

where L_e is linear expansion, L_{90} is the mass of the SYP sample at 90 percent humidity, and L_{50} is the mass of the SYP sample at 50 percent humidity.

Flexural test.—Flexural tests were conducted to determine the strength and stiffness of SYP samples according to ASTM D1037-12 (ASTM 2018a). For each treatment, 10 samples with dimensions of 6.35 mm in thickness, 17.5 mm in width, and 180 mm in length were tested before and after treatments. A Mark-10 universal testing machine (Copiague, New York, USA) with a 500-N load cell was used to apply a downward force at a 3 mm/min rate until the samples fractured. MOE and MOR were calculated using the following equations:

$$E = \frac{L^3\Delta P}{4bd^3\Delta y} \quad (5a)$$

$$R = \frac{3PL}{2bd^2} \quad (5b)$$

where E represents the MOE, R represents the MOR, L represents the length of the sample, P represents the peak load of the load-deflection curve, $\Delta P/\Delta y$ is the slope of the straight-line portion of the linear regression load-deflection curve at 30 percent of the peak load, b is the breadth/width of the sample, and d is the depth/thickness of the sample.

Hardness test.—A Janka ball hardness test was conducted according to ASTM D1037-12 (ASTM 2018a). Samples were prepared by stacking four samples and adhering them to one another using Gorilla Glue (The Gorilla Glue Company, part number 7805601, Sharonville, Ohio, USA) overnight. The samples were placed onto an Instron materials testing system (MTS) fixture modified for the Janka ball hardness test. Penetrations of the sample were made starting at the left end at distance intervals of 51 mm so that one

http://prime-pdf-watermark.prime-prod.pubfactory.com/ | 2024-12-26

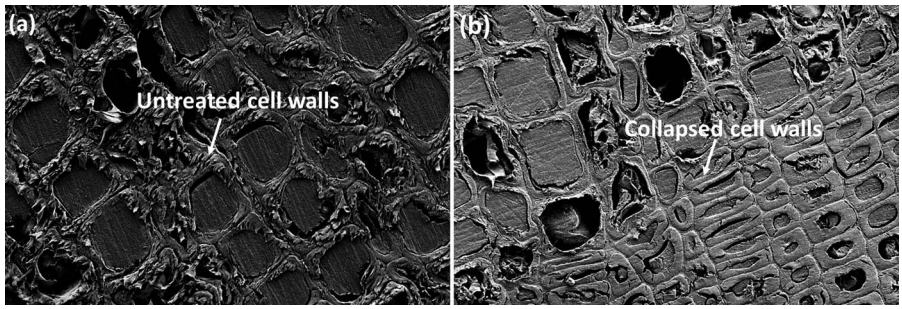

Figure 1.—Field emission scanning electron microscopy of southern yellow pine wood (perpendicular to grain) for (a) an untreated (control, CL) and (b) a treated (3N2AA2CNC) sample.

penetration would not affect the other. Three penetrations were made for each treatment. The load at 5.6-mm penetration was recorded as hardness.

Lab shear test.—To evaluate the adhesive bonding strength of a SYP sample against shear forces, lap shear testing was conducted according to ASTM D2339-98 (ASTM 2018b). Ten SYP strips were cut into a dimension of 6.35 by 17.50 by 76 mm. Each two of these strips were glued together across a 25-mm length and 17.50-mm width. An Instron MTS equipped with a 30-kN load cell was used to separate the glued samples from one another under the application of tensile load at a rate of 1 mm/min. The sample was tested until adhesive failure, where the maximum load was recorded such that the lap shear strength of the SYP could be calculated using the following equation:

$$\tau = \frac{F_{\text{shear}}}{wa} \tag{6}$$

where τ is the shear strength (in MPa), F_{shear} is the shear force required to separate the samples (in N), w is the sample width (in mm), and a is the length of the glue pieces when bonded together (in mm).

Screw withdrawal test.—To evaluate the various loads and ways in which screws fail under tension, the screw withdrawal test was conducted according to ASTM D1037-12 (ASTM 2018a). We used a commercially purchased 16 threads-per-inch type AB wood screw with a root diameter of 3.5 mm and distance intervals of 51 mm so that one penetration would not affect the other at three different points of the sample. The screws were then withdrawn at a rate of 1.5 mm/min until the screw was removed. The peak force required to remove the screw was recorded.

Data analysis

Tukey comparison and Dunnett multiple comparison testing were used ($P < 0.05$) to determine significant differences between individual treatments (Tukey) and treatment groups (Dunnett). The Tukey honestly significant difference comparison test was chosen because of the large number of treatments and its effectiveness in minimizing the likelihood of a type 1 error. This is crucial given the 22 different treatments and variations in wood properties (e.g., density, cut location). Tukey's test, utilizing the t distribution, compares all possible pairs of data sets within a group by calculating a characteristics difference value using the following equation:

$$T_\alpha = q(a,f)\sqrt{\text{MS}_\text{E}} \tag{7}$$

where T_α is the characteristic Tukey's difference value, $q(a, f)$ is a test statistic value based on the t distribution, a is the number of factors or data sets considered in the comparison, and MS_E represents the mean squared error value. Grouping information was assorted by letter and means that did not share a letter were significantly different.

The Dunnett's test is an analysis of variance (ANOVA) procedure designed for comparing multiple treatments with a single control. It assesses if there is a significant difference between the means being compared. This test provides specific confidence levels for each comparison on the basis of a specified family error rate. Compared with the more generalized Tukey pairwise comparison, which considers all types of pairwise comparisons, the Dunnett test addresses the specific case of multiple treatment groups versus a single control group; it yields narrower confidence intervals, increasing precision in the data and reducing the risk of a type 1 error.

Results and Discussion

Treatment effects

Effects of the delignification, along with vacuum–pressure treatment, on the SYP wood were observed using the FESEM. Figure 1a depicts the control sample; it appears to have disrupted cell walls, whereas the cell walls in the treated samples have collapsed because of the delignification and vacuum–pressure treatment. Additionally, the cell walls in the control sample in Figure 1a appear to have a rough, nonuniform structure, whereas the treated sample exhibits a smooth, uniform structure in Figure 1b. A smoother structure in the FESEM suggests lignin removal in the SYP, which is consistent with the findings in the literature (Sun et al. 2009).

Because of the nanoscale dimensions of CNCs, AFM was used to detect the presence of CNCs within the untreated and treated samples through modulus mapping and determine the impact that CNCs have on the mechanical properties of a sample. Previous research in AFM imaging has produced two-dimensional modulus maps with resolutions as fine as 1.5 nm for cellulosic nanomaterials (Wagner et al. 2016). Another study also produced AFM images of wood in a cement environment (Li and Kasal 2022). However, the novelty of the current study lies in generation of three-dimensional maps of surface topography overlaid with monochromatic modulus maps shown for a control sample and a 3N2AA2CNC-treated sample in Figure 2.

http://prime-pdf-watermark.prime-prod.pubfactory.com/ | 2024-12-26

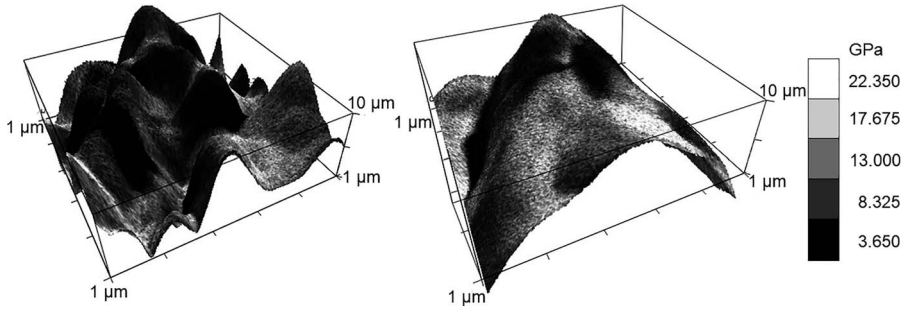

Figure 2.—Three-dimensional atomic force microscopy elastic modulus map over a 1-μm^2 surface area (white = high modulus ~20 GPa, black = low modulus ~3 GPa) of (a) an untreated southern yellow pine (SYP) sample and (b) a 3N2AA2CNC-treated SYP sample.

The detection of CNCs was supported via modulus mapping using the Hertzian contact model, owing to the remarkably higher stiffness of CNCs compared with the SYP. Stiffness was indicated on a monochromatic scale, with darker shades representing lower values (~3 to 8 GPa) and lighter shades denoting higher values (~20 GPa). The untreated maps had an average modulus of 9.639 ± 4.284 GPa, whereas the 3N2AA2CNC-treated sample had an average modulus of 10.351 ± 5.395 GPa, indicating the presence of a higher amount of high-strength CNCs into the treated SYP. The AFM image in Figure 3 depicting CNC-treated wood without delignification revealed an exceptional stiffness, causing the AFM tip to bend backward. Consequently, the indicated highest modulus of 3.37 GPa did not accurately represent the stiffness of that CNC-treated sample.

The resulting FTIR spectra of these treatments were collected with respect to wave numbers from 400 cm^{-1} to 4,000 cm^{-1}, as shown in Figure 4. Nearly identical spectra were observed for all wood formulations. Peaks at around 1,520 to 1,530 cm^{-1} indicated the presence of wood extractives in the form of C=C stretching (Miklečić et al. 2012). The peaks at around 1,680 to 1,690 cm^{-1} represented the presence of unsaturated aromatic acids in the form of C=O stretching (Miklečić et al. 2012). Moreover, peaks at around 3,650 to 3,850 cm^{-1} corresponded to the hydrogen-bonded OH stretching and alcohols (Larkin 2017). A difference in spectrum was observed for the 3N2AA2CNC treatment at around 1,715 to 1,720 cm^{-1}, with an intensified shoulder peak, as depicted in the inset of Figure 3. This peak indicates the presence of ester groups likely the result of Fisher–Speier esterification because peaks around 1,715 to 1,735 cm^{-1} generally correspond to the stretching vibrations of carbonyl esters (-COO-; Larkin 2017). Besides, the successful addition of functional groups to the CNC surface was confirmed by investigating the weight gain in CNC after AA treatment where a 2.29 percent increase in weight was observed. Similar peaks were not detected for the 3N2BA2CNC-treated samples, likely because of the lack of solubility of the BA, inhibiting the esterification of the CNC.

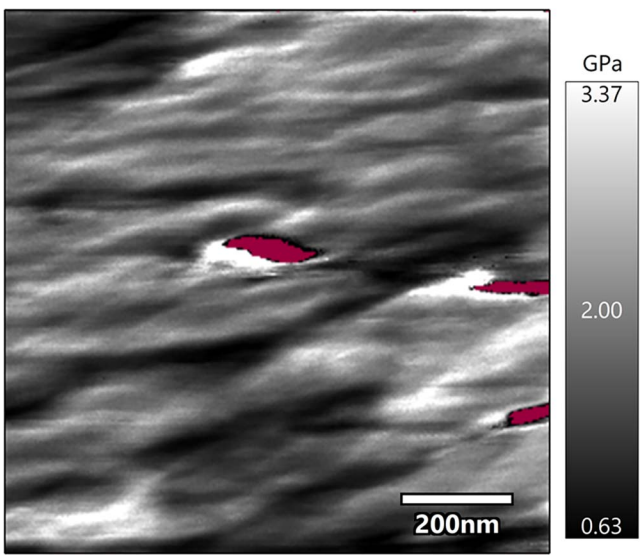

Figure 3.—Stiffness of a sample from force curves generated via atomic force microscopy (AFM). Red inclusions indicate areas of the sample with an extremely high stiffness such that the AFM tip bends backward, indicating the presence of cellulose nanocrystals.

Physical properties

Density.—Density measurements and change in density tests were performed on five samples from each formulation to assess the impacts of delignification and CNC impregnation in the SYP. The delignified samples treated with f-CNC were expected to have the greatest density because of the pores being filled with CNCs, which have a density of 1,600 kg/m^3 (Mariano et al. 2014), compared with commercially sourced SYP, which only has a density of 476 kg/m^3. The present results conform with this expectation with strong evidence showing that CNC caused significantly higher changes in density compared with untreated SYP. Table 2 displays each treatment's mean density, along with their percentage changes in density and Tukey comparison. The 5CNC (i.e., 5% CNC without delignification and esterification) had the greatest observed change in density, and it was the only

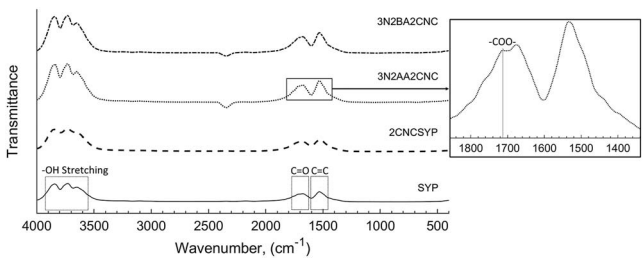

Figure 4.—Fourier transform infrared spectroscopy of untreated and treated (2CNC, 3N2AA2CNC, and 3N2BA2CNC) southern yellow pine wood.

http://prime-pdf-watermark.prime-prod.pubfactory.com/ | 2024-12-26

Table 2.—Physical properties: mean, standard deviation, and Tukey grouping information of seven formulations. Means that do not share a letter are significantly different. CNC = cellulose nanocrystal, N = sodium hydroxide, BA = benzoic acid, AA = acetic acid, CL = control sample.

Treatment	Density (kg/m^3)	Change in density (%)	Water absorption (%)	Thickness swelling (%)	Linear expansion (%)
2CNC	546.93	$21.19^{AB} \pm 1.18$	$35.447^{BC} \pm 0.86$	$9.450^{AB} \pm 0.82$	$0.398^{A} \pm 0.061$
5CNC	600.52	$29.96^{A} \pm 4.61$	$41.141^{A} \pm 1.76$	$10.398^{A} \pm 1.22$	$0.484^{A} \pm 0.070$
3N2AA2CNC	575.59	$23.58^{AB} \pm 3.52$	$31.41^{C} \pm 1.58$	$5.205^{C} \pm 0.70$	$0.317^{A} \pm 0.075$
3N2AA5CNC	548.55	$16.67^{AB} \pm 1.55$	$39.45^{AB} \pm 1.27$	$6.440^{BC} \pm 0.63$	$0.341^{A} \pm 0.057$
3N2BA2CNC	548.55	$26.19^{AB} \pm 4.61$	$30.25^{C} \pm 1.82$	$6.443^{ABC} \pm 0.10$	$0.343^{A} \pm 0.067$
3N2BA5CNC	587.00	$24.71^{AB} \pm 1.37$	$38.32^{AB} \pm 1.38$	$7.256^{ABC} \pm 0.39$	$0.345^{A} \pm 0.047$
CL	476.50	$0^{B} \pm 0.00$	$36.85^{AB} \pm 1.74$	8.258 ± 0.53	$0.344^{A} \pm 0.066$

treatment significantly different from the control sample according to the Tukey comparison correction.

Because the Tukey comparison test produced overlapping letters, the Dunnett multiple comparison test was conducted to further assess the effects of treatments. Dunnett analysis also revealed that the CNC concentration had a significant effect, particularly with both 2 and 5 percent concentrations of added CNCs. However, the BA and AA f-CNCs did not appear to have a statistically significant impact on the density of the material. Besides, the delignification process by NaOH has been observed to have a reducing effect on the density of the material (Kuai et al. 2022). Therefore, it is plausible that the slight reduction in lignin mass from the NaOH treatment was counterbalanced by the introduction of high-density CNC impregnation, potentially leading to the observed increase in density in the delignified and CNC-impregnated SYP. The present results are compared with similar research involving the impregnation of other materials, such as nanoaluminum oxide and sodium silicate, into wood, and the previous research also demonstrated an increase in wood density after impregnation (Taghiyari et al. 2017, Kuai et al. 2022).

Water absorption and thickness swelling.—The affinity to water of treated and untreated SYP samples was determined by mass and thickness swelling of five samples from each formulation. The results from Tukey comparison tests in Table 2 show that SYP treated with 5 percent CNC had the highest water absorption (41.41%), whereas samples delignified and treated with BA f-CNC had the lowest (30.25%). Dunnett's test found that water absorption increases slightly from 36.85 to 41.14 percent at the 5 percent CNC concentrations, whereas NaOH treatment led to a decrease in water absorption from 38.39 to 34.76 percent. Another observation noted that neither AA nor BA had an effect in reducing the water absorption of CNCs. Similar trends in the effect of CNC impregnation, delignification, and CNC functionalization were observed for the thickness swelling behavior of the SYP, as shown in Table 2.

The increased water absorption and thickness swelling of the higher-CNC concentrated SYP sample is due to the hydrophilic nature of the CNCs (Shikata and Okuzono 2013). The reduction in water absorption and thickness swelling resulting from the NaOH treatment can be attributed to the delignification process, which promotes the collapse of cell walls, as observed in Figure 1b. This collapse, in turn, hinders the movement of water within the cells (Wang et al. 2021, Liang et al. 2022).

Linear expansion.—Linear expansion testing was conducted to determine the relative expansion of SYP in the lengthwise dimension due to changes in environmental humidity. Both Tukey and Dunnett analyses indicated no significant differences between any of the formulas. The lack of notable differences combined with the drastic value changes observed in some groups in the Dunnett model led to the development of a model-reduced ANOVA, removing AA to discount its effects as it had the highest *P* value. The test indicated that both NaOH and CNCs caused a minor increase in the linear expansion. A challenge in detecting notable increases in linear expansion likely arises from the notable variation among the samples, which is evident in Table 2 because of high coefficient-of-variation values observed.

Mechanical properties

Flexural behavior.—Flexural tests were conducted on 10 samples from each formulation to determine the stiffness and bending strengths of treated and untreated SYP samples. The MOR represents the maximum flexural strength the SYP undergoes before failure. Figure 5 shows the MOR values of seven formulations, their statistical means, and Tukey comparison. The results indicate that all treatments differed significantly and increased relative to the control, as they did not share a letter except for the 3N2BA5CNC treatment, which shared the letter C with the control. Moreover, the 2CNC treatment had the highest observed MOR of 171.12 MPa, superior to that of Live Oak by a difference of 35 percent (Ross 2021). Because multiple treatments shared the same letters, the Dunnett test was also conducted for further analysis of the effects of each treatment.

According to the Dunnett test, the inclusion of CNCs resulted in a noteworthy increase in MOR, from 97.18 MPa to 147.54 MPa. Conversely, the addition of BA led to a significant decrease in MOR, from 135.55 MPa to 123.09 MPa.

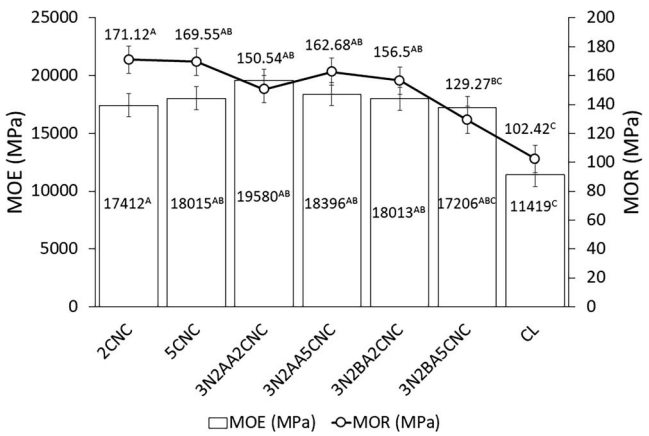

Figure 5.—Flexural test results of seven formulations including the control with data labels and Tukey grouping information. MOE = modulus of elasticity; MOR = modulus of rupture.

http://prime-pdf-watermark.prime-prod.pubfactory.com/ | 2024-12-26

Table 3.—Fastener withdrawal, hardness, and lap shear properties of the untreated and treated southern yellow pine with mean, standard deviation, and Tukey grouping information. CNC = cellulose nanocrystals, N = sodium hydroxide, BA = benzoic acid, AA = acetic acid, CL = control sample.

Formulation	Screw withdrawal (N)	Nail withdrawal (N)	Hardness (N)	Lap shear (MPa)
2CNC	$907^{D} \pm 109.49$	$41.33^{BC} \pm 9.61$	$3{,}437^{AB} \pm 43.3$	$3.64^{B} \pm 0.14$
5CNC	$894^{D} \pm 28.91$	$32^{C} \pm 2.65$	$3{,}044^{AB} \pm 70.6$	$4.31^{A} \pm 0.14$
3N2BA2CNC	$1{,}100^{BCD} \pm 16.86$	$56^{AB} \pm 19.1$	$2{,}502^{C} \pm 168.6$	$1.84^{E} \pm 0.10$
3N2BA5CNC	$1{,}298^{AB} \pm 11.01$	$49.33^{ABC} \pm 2.52$	$2{,}822^{CD} \pm 72.4$	$2.48^{D} \pm 0.10$
3N2AA2CNC	$1{,}122^{BC} \pm 43.82$	$66^{A} \pm 25.2$	$3{,}598^{A} \pm 218$	$1.88^{E} \pm 0.19$
3N2AA5CNC	$1{,}373^{A} \pm 118.68$	$54.67^{ABC} \pm 8.5$	$2{,}996^{D} \pm 205$	$3.06^{C} \pm 0.05$
CL	$947^{CD} \pm 45.00$	$42.67^{BC} \pm 3.06$	$2{,}814^{CD} \pm 110.1$	$3.03^{C} \pm 0.09$

A possible reason for the decrease in MOR by BA is the lack of dispersion of the BA f-CNC, resulting from its limited solubility, which in turn hinders nanodispersion during ultrasonication (Jasmani et al. 2016). On the other hand, an increase from 124.74 MPa to 133.91 MPa was observed with AA. This is likely due to the acetylation of CNCs improving their dispersion and crystallinity throughout the SYP (Tang et al. 2013). A previous study also reported increases in MOR due to impregnating poplar wood with high MOR materials such as CNCs and nanoaluminum oxide because of its superior mechanical strength (Taghiyari et al. 2017, Luo et al. 2022).

The MOE represents the sample's stiffness during initial loading before unrecoverable deformation occurs. Figure 4 shows the MOE values and Tukey grouping information of seven formulations, including the control. The results indicate that the samples treated with 3N2AA2CNC had the highest MOE, whereas those treated with 3N2BA5CNC had the lowest. Additionally, the MOE of 3N2AA2CNC-treated samples surpassed that of Live Oak, showing a remarkable 43 percent increase (Ross 2021). Furthermore, delignified and AA functionalized treatment with a 2 percent CNC concentration led to higher MOE of SYP wood than the same treatment with a 5 percent CNC concentration. Because of the sharing of multiple letters in the Tukey comparison test among several samples, the Dunnett multiple-comparison test was conducted to verify treatment effects.

The Dunnett test indicated that CNC treatment resulted in a significant increase in MOE, from 12,057 to 18,119 MPa, which is attributed to the high stiffness of the impregnated CNCs, as observed in Figure 2. Additionally, a slight decrease in MOE was observed at the 5 percent CNC concentration. This suggests the possibility that CNCs might have started to agglomerate on the surface because of the increased viscosity of the solution, rather than penetrating the wood cell. The increase in viscosity of the CNC solution is attributed to the formation of hydrogen bonds, a consequence of the surface hydroxyl groups within the structure of CNCs. For similar reason, a previous study reported a decrease in the hardness of treated material at higher solution concentrations of CNCs (Mohamed et al. 2018). However, AA treatment of CNCs resulted in improved MOE because the treatment led to functionalization of CNCs, avoiding the hydroxyl interactions and increasing the interfacial compatibility with the wood (Rana et al. 2021).

Fastener withdrawal.—Fastener withdrawal tests were conducted using five samples from each formulation to determine the maximum force required for the withdrawal of screw and nail. Table 3 presents the screw-and-nail withdrawal values and Tukey grouping information of seven formulations, including the control. It was determined that the 3N2AA5CNC treatment resulted in the highest screw withdrawal force, whereas the 5CNC sample exhibited the lowest screw withdrawal force. The nail withdrawal force was also higher for the delignified and f-CNC-impregnated wood than the CNC-impregnated wood alone, and the highest nail withdrawal was for the 3N2AA2CNC treatment. Hence, it can be inferred that the AA functionalization of CNCs improved the interface between the wood and the fastener because of their better dispersion and esterification, as found from the FTIR analysis in Figure 3.

Besides, Dunnett multiple comparison tests provided strong evidence that the delignification via NaOH led to a significant increase in the screw withdrawal force of SYP, from 868 N to 1,262 N, and an increase in the nail withdrawal force, from 38.83 N to 57.16 N. The increase is likely because of the compression of the cell walls by delignification and enhanced penetration of CNC into the wood, resulting in a more uniform interface between wood and fastener. This possibility is supported by previous research where delignification alone reduced poplar's dimensional stability and led to cell wall collapse (Yang et al. 2019, Fotie et al. 2020). However, when combined with furfuryl resin impregnation, it resulted in greater microstructure uniformity (Yang et al. 2019).

Hardness.—Hardness tests were conducted to measure resistance to localized plastic deformation of a wood sample. Table 3 presents the statistical means and Tukey comparison of the hardness. These data indicate strong evidence that the 3N2AA2CNC and 2CNC treatments significantly differ from the control sample because of them not sharing a letter with the control treatment. The Dunnett comparison test was used to further verify the efficacy of the treatment groups. It was found through the Dunnett comparison test that BA functionalization of CNCs caused a decrease from 3,110 N to 2,653 N compared with AA in the hardness of SYP. A possible cause of this is a lack of dispersion of the BA-functionalized CNCs due to their lack of solubility, thus hindering nanodispersion during ultrasonication (Jasmani et al. 2016). The CNCs were also observed to have caused a significant increase in hardness. The means obtained via the Dunnett test for the CNCs found a significant increase between CNC level 0 (2,597 N) and levels 2 and 5 (2,970 N and 3,078 N, respectively). However, the increase in the concentration of CNCs from 2 to 5 wt. percent does not increase as greatly as from 0 to 2 wt. percent. A possible cause for this is the increased viscosity of the 5 percent CNC solution, leading to localized clusters of CNCs on the surface of the SYP. Increase in hardness can also be attributed to densification of

http://prime-pdf-watermark.prime-prod.pubfactory.com/ | 2024-12-26

wood because of vacuum treatment and impregnation of CNCs into the lumen, as seen in FESEM Figures 1a and 1b. A previous study on the microhardness of CNCs on polyester found that on the surface of the polyester, 4 percent CNCs had a slightly greater hardness compared with 6 percent CNCs (Mohamed et al. 2018).

Lap shear.—Lap shear tests on SYP samples evaluated adhesive bonding strength. Table 3 displays statistical means and Tukey comparison values for seven formulations, including the control. The 5CNC treatment exhibited the highest lap shear, whereas the 3N2BA2CNC showed the lowest. The increase is attributed to CNCs' short (<100 nm), rigid, and rodlike morphology, which was reported to enhance epoxy adhesive strength as well (Lee et al. 2012). The presence of CNCs in wood possibly had a synergistic effect, improving shear strength by reinforcing the wood–adhesive interface. The Dunnett test confirmed the significant effects on lap shear for CNCs, NaOH, and AA, as they did not share a letter. BA was excluded because of its failure of the regression test. NaOH led to an observed decrease in lap shear, possibly due to its caustic nature affecting wood surface fiber (Dimitriou et al. 2018, Rajeshkumar et al. 2021). AA treatment improved lap shear, likely because of AA esterification of CNCs and enhanced dispersion through acetylation (Tang et al. 2013, Arrieta et al. 2014). This improvement is supported by research showing that esterified CNCs increased lap shear in various plastic films (Fotie et al. 2020). BA showed minimal effect on lap shear because of its insolubility, hindering nanodispersion during ultrasonication (Jasmani et al. 2016).

Conclusion

The objective of this study encompassed the optimization and validation of an efficient process for impregnating wood with f-CNCs, along with the identification of critical variables influencing CNC impregnation. Furthermore, the investigation delved into microstructural and compositional changes within the wood after CNC impregnation. Finally, the study sought to comprehensively evaluate the resulting alterations in the physical and mechanical properties of the wood postimpregnation with CNCs. The first objective was achieved using an alkali delignification technique, enhancing wood porosity for improved CNC impregnation. The delignification was followed by ultrasonication, which effectively impregnated the wood with CNCs and dispersed the CNC nanosolution uniformly. Subsequently, a vacuum–pressure impregnation process was used to remove air pockets and introduce additional CNCs into the wood.

The second objective was completed through FESEM, AFM, and FTIR. FESEM analyzed microstructural and morphological changes, revealing cell wall collapse and lignin removal in the delignified SYP. AFM detected CNC presence via modulus mapping and provided surface topography data. FTIR identified ester groups in the f-CNC-modified SYP. The third objective encompassed ASTM D1037-12 and ASTM D2339-98 tests. These revealed improved physical properties, including reduced water absorption and thickness swelling due to cell wall collapse and enhanced mechanical properties resulting from the CNC impregnation and functionalization.

This study demonstrates that combining SYP wood's delignification and densification by CNC significantly improves mechanical properties, yielding a 67 percent increase in MOR and a 71 percent increase in MOE. Delignification enhances fastener withdrawal properties without substantial impact on moisture absorption. Vacuum–pressure impregnation with CNCs yields positive effects, including increased resistance in fastener withdrawal, MOR, MOE, and lap shear strength. These results suggest that adding CNCs to SYP could yield a high-strength material suitable for architectural and engineering applications, such as cross-laminated timber and hardwood flooring. The optimal treatment was found to be 3N2AA2CNC.

Moreover, a novel AFM method for detecting CNCs was developed using a box cutter for sample preparation, reducing the risk of resin contamination and the need for surface polishing. Future work includes additional testing to determine wood impregnation efficiency, industrialization of the impregnation process (e.g., use in cross-laminated timber), and finding a method for smooth SYP sample cutting to provide larger area maps in AFM. In addition, alternative impregnation techniques such as the Lowry method may be explored for more efficient impregnation of CNCs into the wood.

Acknowledgment

This work is supported by the U.S. Department of Agriculture National Institute of Food and Agriculture grant no. 13058620, award 2021-67022-3400.

Literature Cited

Abraham, J., B. Jose, A. Jose, and S. Thomas. 2020. Characterization of green nanoparticles from plants. *In:* Phytonanotechnology. N. Thajuddin and S. Mathew (Eds.). Elsevier, Amsterdam, the Netherlands. pp. 21–39. https://doi.org/10.1016/B978-0-12-822348-2.00002-4

Ameh, J., A. Soyingbe, and O. Oyediran. 2019. Acceptability and use of innovative bamboo products for the construction of residential buildings in Nigeria. *Int. J. Technol*. 10(4):648–656. https://doi.org/10.14716/ijtech.v10i4.2574

Arrieta, M. P., E. Fortunati, F. Dominici, E. Rayón, J. López, and J. M. Kenny. 2014. Multifunctional PLA–PHB/cellulose nanocrystal films: Processing, structural and thermal properties. *Carbohydr. Polym*. 107:16–24. https://doi.org/10.1016/j.carbpol.2014.02.044

ASTM International 2018a. Standard test methods for evaluating properties of wood-base fiber and particle panel materials. ASTM D1037-12. ASTM International, West Conshohocken, Pennsylvania.

ASTM International 2018b. Standard test method for strength properties of adhesives. ASTM D2339-98. ASTM International, West Conshohocken, Pennsylvania.

Brandner, R., G. Flatscher, A. Ringhofer, G. Schickhofer, and A. Thiel. 2016. Cross laminated timber (CLT): Overview and development. *Eur. J. Wood Wood Prod*. 74:331–351. https://doi.org/10.1007/s00107-015-0999-5

Briggs, D. 2010. Enhancing forest value productivity through fiber quality. *J. Forestry* 108(4):174–182. https://doi.org/10.1093/jof/108.4.174

Chanda, S. and D. S. Bajwa. 2021. A review of current physical techniques for dispersion of cellulose nanomaterials in polymer matrices. *Rev. Adv. Mater. Sci*. 60(1):325–341. https://doi.org/10.1515/rams-2021-0023

Dimitriou, A., M. D. Hale, and M. J. Spear. 2018. The effect of pH on surface activation of wood polymer composites (WPCs) with hydrogen peroxide for improved adhesion. *Int. J. Adhes*. 85:44–57. https://doi.org/10.1016/j.ijadhadh.2018.05.012

Fotie, G., S. Gazzotti, M. A. Ortenzi, and L. Piergiovanni. 2020. Implementation of high gas barrier laminated films based on cellulose nanocrystals for food flexible packaging. *Appl. Sci*. 10(9):3201 . https://doi.org/10.3390/app10093201

Frey, M., D. Widner, J. S. Segmehl, K. Casdorff, R. Keplinger, and I. Burgert. 2018. Delignified and densified cellulose bulk materials with excellent tensile properties for sustainable engineering. *ACS Appl. Mater. Interfaces* 10(5):5030–5037. https://doi.org/10.1021/acsami.7b18646

http://prime-pdf-watermark.prime-prod.pubfactory.com/ | 2024-12-26

Habibi, Y., L. A. Lucia, and O. J. Rojas. 2010. Cellulose nanocrystals: Chemistry, self-assembly, and applications. *Chem. Rev.* 110(6):3479–3500. https://doi.org/10.1021/cr900339w

Jasmani, L., S. Eyley, C. Schütz, H. Van Gorp, S. De Feyter, and W. Thielemans. 2016. One-pot functionalization of cellulose nanocrystals with various cationic groups. *Cellulose* 23(6):3569–3576. https://doi.org/10.1007/s10570-016-1052-5

Kargarzadeh, H., M. Mariano, J. Huang, N. Lin, I. Ahmad, A. Dufresne, and S. Thomas. 2017. Recent developments on nanocellulose reinforced polymer nanocomposites: A review. *Polymer* 132:368–393. https://doi.org/10.1016/j.polymer.2017.09.043

Khakalo, A., A. Tanaka, A. Korpela, and H. Orelma. 2020. Delignification and ionic liquid treatment of wood toward multifunctional high-performance structural materials. *ACS Appl. Mater. Interfaces* 12(20):23532–23542. https://doi.org/10.1021/acsami.0c02221

Kollmann, F. F., E. W. Kuenzi, and A. J. Stamm. 2012. Principles of Wood Science and Technology: II Wood Based Materials. Springer Science & Business Media, Berlin.

Kuai, B., Z. Wang, J. Gao, J. Tong, T. Zhan, Y. Zhang, J. Lu, and L. Cai. 2022. Development of densified wood with high strength and excellent dimensional stability by impregnating delignified poplar by sodium silicate. *Constr. Build. Mater*. 344:128282. https://doi.org/10.1016/j.conbuildmat.2022.128282

Laks, P. E. 2008. Wood preservative fungicides and the American Wood Preservers' Association use category system. *ACS Symp. Ser*. 13:228–240. https://doi.org/10.1021/bk-2008-0982.ch013

Larkin, P. 2017. Infrared and Raman Spectroscopy: Principles and Spectral Interpretation. 2nd ed. Elsevier, New York.

Lee, K. Y., T. Tammelin, K. Schulfter, H. Kiiskinen, J. Samela, and A. Bismarck. 2012. High performance cellulose nanocomposites: Comparing the reinforcing ability of bacterial cellulose and nanofibrillated cellulose. *ACS Appl. Mater. Interfaces* 4(8):4078–4086. https://doi.org/10.1021/am300852a

Li, J. and B. Kasal. 2022. The immediate and short-term degradation of the wood surface in a cement environment measured by AFM. *Mater. Struct*. 55(7):179. https://doi.org/10.1617/s11527-022-01988-8

Liang, Y., G. Zheng, C. Xia, S. Zuo, S. Ge, R. Yang, X. Ma, B. Fei, J. Li, C. K. Cheng, and S. Y. Kim. 2022. Synthesis of ultra-high strength structured material from steam-modified delignification of wood. *J. Clean. Prod*. 351:131531. https://doi.org/10.1016/j.jclepro.2022.131531

Luo, H., R. Si, J. Liu, P. Li, Y. Tao, X. Zhao, and H. Chen. 2022. Preparing the reinforced wood via embedding cellulose nanocrystals (CNC) into delignified fast-growing wood followed by densification. *Cellulose* 29(13):7377–7396. https://doi.org/10.1007/s10570-022-04727-y

Mariano, M., N. El Kissi, and A. Dufresne. 2014. Cellulose nanocrystals and related nanocomposites: Review of some properties and challenges. *J. Polym. Sci. B Polym. Phys*. 52(12):791–806. https://doi.org/10.1002/polb.23490

Miklečić, J., N. Španić, and V. Jirouš-Rajković. 2012. Wood color changes by ammonia fuming. *Bio. Resour*. 7(3):3767–3778.

Mohamed, Y. S., H. El-Gamal, and M. M. Y. Zaghloul. 2018. Micro-hardness behavior of fiber reinforced thermosetting composites embedded with cellulose nanocrystals. *Alex. Eng. J*. 57(4):4113–4119. https://doi.org/10.1016/j.aej.2018.10.012

Nepal, P., C. M. Johnston, and I. Ganguly. 2021. Effects on global forests and wood product markets of increased demand for mass timber. *Sustainability* 13(24):13943. https://doi.org/10.3390/su132413943

Nikolic, M., J. M. Lawther, and A. R. Sanadi. 2015. Use of nanofillers in wood coatings: A scientific review. *J. Coat. Technol. Res*. 12:445–461. https://doi.org/10.1007/s11998-015-9659-2

Qian, M., H. Lei, E. Villota, W. Mateo, Y. Zhao, E. Huo, Q. Zhang, X. Lin, and Z. Huang. 2019. Optimization of delignification from Douglas fir sawdust by alkaline pretreatment with sodium hydroxide and its effect on structural and chemical properties of lignin and pyrolysis products. *Bioresour. Technol. Rep*. 8:100339. https://doi.org/10.1016/j.biteb.2019.100339

Rajendran, N., T. Runge, R. D. Bergman, P. Nepal, and C. Houtman. 2023. Techno-economic analysis and life cycle assessment of cellulose nanocrystals production from wood pulp. *Bioresour. Technol*. 377:128955. https://doi.org/10.1016/j.biortech.2023.128955

Rajeshkumar, G., V. Hariharan, S. Indran, M. R. Sanjay, S. Siengchin, J. P. Maran, N. A. Al-Dhabi, and P. Karuppiah. 2021. Influence of sodium hydroxide (NaOH) treatment on mechanical properties and morphological behaviour of Phoenix sp. fiber/epoxy composites. *J. Polym. Environ*. 29:765–774. https://doi.org/10.1007/s10924-020-01921-6

Rana, A. K., E. Frollini, and V. K. Thakur. 2021. Cellulose nanocrystals: Pretreatments, preparation strategies, and surface functionalization. *Int. J. Biol. Macromol*. 182:1554–1581. https://doi.org/10.1016/j.ijbiomac.2021.05.119

Rasouli, D., M. Bahmani, and M. Humar. 2017. Impregnability of *Paulownia* and *Populus* wood with copper based preservatives. *Drv. Ind*. 68(3):211–218. https://doi.org/10.5552/drind.2017.1701

Reza, M., E. Kontturi, A. S. Jääskeläinen, T. Vuorinen, and J. Ruokolainen. 2015. Transmission electron microscopy for wood and fiber analysis—A review. *BioResources* 10(3):6230–6261.

Ross, R. J. 2021. Wood handbook: wood as an engineering material. General Technical Report FPL-GTR-282. US Department of Agriculture Forest Service, Forest Products Laboratory, Madison, Wisconsin. 543 pp.

Sandberg, D., Kutnar, A. and Mantanis, G. 2017. Wood modification technologies-a review. *Iforest-Biogeosciences and forestry*. 10(6): p.895. https://doi.org/10.3832/ifor2380-010

Shikata, T. and Okuzono, M. 2013. Are all polar molecules hydrophilic? Hydration numbers of ketones and esters in aqueous solution. *J. Phys. Chem. B*. 117(25): 7718–7723. https://doi.org/10.1021/jp4029968

Shojaeiarani, J., D. S. Bajwa, and N. M. Stark. 2018. Green esterification: A new approach to improve thermal and mechanical properties of poly (lactic acid) composites reinforced by cellulose nanocrystals. *J. Appl. Polym. Sci*. 135(27):46468. https://doi.org/10.1002/app.46468

Sun, N., M. Rahman, Y. Qin, M. L. Maxim, H. Rodríguez, and R. D. Rogers. 2009. Complete dissolution and partial delignification of wood in the ionic liquid 1-ethyl-3-methylimidazolium acetate. *Green Chem*. 11(5):646–655. https://doi.org/10.1039/B822702K

Taghiyari, H. R., G. Rassam, and K. Ahmadi-DavazdahEmam. 2017. Effects of densification on untreated and nano-aluminum-oxide impregnated poplar wood. *J. Forest Res*. 28(2):403–410. https://doi.org/10.1007/s11676-016-0321-3

Tang, L., B. Huang, Q. Lu, S. Wang, W. Ou, W. Lin, and X. Chen. 2013. Ultrasonication-assisted manufacture of cellulose nanocrystals esterified with acetic acid. *Bioresour. Technol*. 127:100–105. https://doi.org/10.1016/j.biortech.2012.09.133

Wagner, R., R. J. Moon, and A. Raman. 2016. Mechanical properties of cellulose nanomaterials studied by contact resonance atomic force microscopy. *Cellulose* 23:1031–1041. https://doi.org/10.1007/s10570-016-0883-4

Wang, J., J. Liu, J. Li, and J. Y. Zhu. 2021. Characterization of microstructure, chemical, and physical properties of delignified and densified poplar wood. *Materials* 14(19):5709. https://doi.org/10.3390/ma14195709

Yang, T., J. Cao, and E. Ma. 2019. How does delignification influence the furfurylation of wood? *Ind. Crops Prod*. 135:91–98. https://doi.org/10.1016/j.indcrop.2019.04.019

http://prime-pdf-watermark.prime-prod.pubfactory.com/ | 2024-12-26